AIAA Propulsion and Energy Forum
July 27-29, 2015, Orlando, FL
51st AIAA/SAE/ASEE Joint Propulsion Conference

10.2514/6.2015-3721

Characterization of Discharge Uniformity and Performance via Simulated Beam Extraction of a 65 cm Annular Ion Engine

Neil A. Arthur* and John E. Foster†
University of Michigan, Ann Arbor, MI, 48109, USA

Michael J. Patterson‡ and Robert E. Thomas§
NASA Glenn Research Center, Cleveland, OH, 33135, USA

Jason A. Young¶ and Mark W. Crofton‖
The Aerospace Corporation, El Segundo, CA, 90245, USA

The annular ion engine concept consists of a cylindrical ion thruster with a centrally located stalk that provides increased anode area. The increased electron collection area allows for increased discharge plasma current, and thus high power operation. The central stalk also provides support for the ion optics, allowing for larger beam area and scale up potential. Discharge performance of a 42 cm annular ion engine has previously been studied. Here, the discharge uniformity of a 65 cm annular ion engine during simulated beam extraction is assessed using three diagnostics: Faraday probes, Langmuir probes, and a fast camera. The percent uniformity was found to vary from 89.8% to 97.4% for discharge powers under 1.5 kW. The data presented herein demonstrates the feasibility of scalability of the annular ion engine.

*PhD candidate, Nuclear Engineering and Radiological Sciences, 2355 Bonisteel Blvd., AIAA student member
†Professor, Nuclear Engineering and Radiological Sciences, 2355 Bonisteel Blvd., AIAA member
‡Senior Technologist, Power and In-Space propulsion Division, 2100 Brookpark Rd./MS 301-3, AIAA senior member
§Research Engineer, Propulsion and Propellants Branch, 21000 Brookpark Rd./MS 301-3, AIAA member
¶Member of Technical Staff, Space Materials Laboratory, P.O. Box 92957 M2-341, AIAA member
‖Senior Scientist, Space Materials Laboratory, P.O. Box 92957 M2-341, AIAA senior member

Nomenclature

A_b = beam area
$\vec{B}$ = magnetic field
d_s = screen grid aperture diameter
I_b = beam current
I_D = discharge current
$j_{b,max}$ = button probe line maximum current density
$j_{b,min}$ = button probe line minimum current density
l_e = electrode spacing
l_g = grid spacing
M = ion mass
m = electron mass
P_D = discharge power
q = electrical charge
t_s = screen grid thickness
$v_\parallel$ = electron velocity parallel to $\vec{B}$
$v_\perp$ = electron velocity perpendicular to $\vec{B}$
$v_{\nabla \vec{B}}$ = Grad B drift velocity
v_C = curvature drift velocity
v_D = combined drift velocity
V_D = discharge voltage
V_b = beam voltage
γ = thrust-loss correction factor
ϵ_0 = vacuum permittivity
Ω = cyclotron frequency

I. Introduction

GRIDDED ion thrusters offer the higest specific impulse range of any of the electric propulsion technologies. Its nominal electrical efficiency also exceeds the current state of the art of mature electric propulsion devices. At present this engine technology has seen application on a number of space science missions and over one hundred communication satellite missions (station keeping). These engines have conventionally been operated at low thrust to power for missions of interest, owing to power limitations or simply the desire to maximize engine lifetime. Ion engines are capable of operating at high thrust densities. Indeed, in the laboratory setting, engines have operated at thrust densities near 10 N/m^2.[1] Ion engine current density is limited by the Child-Langmuir law for space charge flow, which represents a fundamental upper limit. The thrust density of electrostatic ion thrusters is given by:

$$F_A = \gamma \sqrt{\frac{2M}{q}} \frac{I_b \sqrt{V_b}}{A_b} \tag{1}$$

where F_A is the thrust per unit area, I_b is the beam current, V_b is the beam voltage, M is the ion mass, q is the ion charge, A_b is the beam area and γ is the thrust-loss correction factor. The quantity I_b/A_b is the ion beam current density, J_b. The thrust density is maximized as γ approaches unity and J_b is maximized. These factors are limited by the extraction capability of the ion optics and the source production of ions. The space charge limited current density as described by the Child-Langmuir law is:

$$J_b = \frac{4}{9} \epsilon_0 \sqrt{\frac{2q}{M_i}} \frac{V^{3/2}}{l_e^2} \tag{2}$$

where l_e is the electrode spacing. For ion optics the beam current density has the dependence

$$J_b \propto \frac{V_t^{3/2}}{\left(l_g + t_s\right)^2 + \left(d_s/2\right)^2} \tag{3}$$

where l_g is the grid spacing, t_s is the screen grid thickness, and d_s is the screen grid aperture diameter. The total voltage, V_t has a practical limit such that shorting does not occur between grids. This practical limit is determined by the span-to-gap ratio, which for conventional ion thrusters is ∼650-700.

Interestingly, state of the art ion engines operate well below this limit. While in the past, beam current was artificially constrained due to lifetime requirements and limited power available, the availability of energy, via high power solar arrays and NASA's interest in high power solar electric propulsion supporting human missions, has renewed interest in extending the operating range of gridded ion thruster. Interestingly, it has been shown that conventional ring cusp ion engines are source limited at high discharge currents; that is, for a given geometry there is an operational upper limit to the discharge current before the IV response becomes resistive or simply unstable. It is believed that this limitation is associated with the effective surface area defined by the magnetic cusps. Simply put, the available surface area is not capable of collecting additional current without an increase in voltage or the presence of an instability to scatter electrons to the anode surface. Increasing the size of the engine is another approach to increasing overall beam current and thus thrust. From an engineering standpoint, the span-to-gap considerations for high perveance ion optics limits grids to 50 cm in diameter.

The annular ion engine concept is a nonconventional approach to circumventing the aforementioned technical challenges. The annular ion engine concept, described in detail elsewhere, features a cylindrical engine geometry with a centralized cylindrical stalk.[2–4] The cylindrical stalk serves two roles: 1) provides additional anode collection surface area and 2) serves as a mounting central support surfafce to accommodate large area ion optics. In this regard, the engine is capable of approaching the Child-Langmuir limit for a given geometry. The annular engine technology addresses the practical limiting factors in Eqs. (1)-(3). Additionally, with the central support, the engine has tremendous growth potential well into the 100's kW range. Presented herein are preliminary discharge tests of a 65 cm variant of the annular ion engine. This engine has the projected capacity to operate at full power up to 60 kW. The discharge data presented herein follow previous tests conducted on a 42 cm variant demonstrating the scalability of the technology. The annular geometry can allow for operation with increased discharge currents, thereby increasing thrust density by up to 3x.[2]

Presented here is a overview of a preliminary simulated beam extraction test of the 65 cm annular engine. The chief focus of the effort was to assess discharge uniformity and stability over a range of operating conditions. Because the engine utilizes a single cathode asymmetrically placed in the discharge chamber, the uniformity in particularly is of great interest. To assess uniformity, Faraday probes were affixed on an ion collector plate at the exit plane of the device. Three Langmuir probes were used to assess discharge plasma properties. Additionally, a fast frame-rate camera was used to investigate startup dynamics and instabilities.

II. Experimental Apparatus

A. Vacuum Facility

Characterization of the discharge chamber was carried out at The Aerospace Corporation's Electric Propulsion 2 (EP2) space simulation facility. EP2 is a cylindrical chamber with a 2.4 m diameter by 9.4 m length, with a pumping speed of ∼200 kL/s on xenon.

B. Test Article

The test article investigated is a 65 cm annular geometery ion (AGI) thruster. The outer diameter of the annulus is 65 cm, and the inner diameter of the annulus is 36 cm. The test article will be referred to as AGI-Engine 6536, which essentially specifies the annulus shaped discharge chamber. The engine was fabricated at NASA Glenn Research Center (GRC). The AGI-Engine 6536 was sized to process 60 kW input power, with a beam area 2x large than NEXT and an anode area 4x larger than NEXT. During initial discharge testing the thruster input power was limited by the current capacity of the discharge power supply. For simulated beam extraction, a perforated plate was placed at the discharge chamber exit plane. The plate was biased

to cathode potential. Testing up to 1.5 kW was carried out. Higher power testing was limited by the power console and an intermittent thermally-induced short, which developed between the perforated grid plate and the discharge chamber.

C. Electrostatic Probes

The engine was operated in discharge only mode using simulated beam extraction.[5] The spatial uniformity of the annular discharge plasma was measured using 13 Faraday probes mounted on the extraction grid. Each planar probe consists of 6.4 mm diameter molybdenum discs. The relative locations of the probes are illustrated in Fig. 1. Probe line "A" consisted of five probes at the 12 o'clock position, with the middle probe located directly downstream of the cathode orifice. Lines "B" and "C" each consist of four probes 120°apart from line "A". Three Langmuir probes were also utilized in this study. The three Langmuir probes are also spaced 120°apart. The approximate clock position of each Langmuir probe is designated as a green diamond in Fig. 1a. Each Langmuir probe extended axially halfway into the discharge chamber. This probe configuration allowed for determination of the plasma properties and uniformity across the annulus, including an interrogation line that includes the cathode axis.

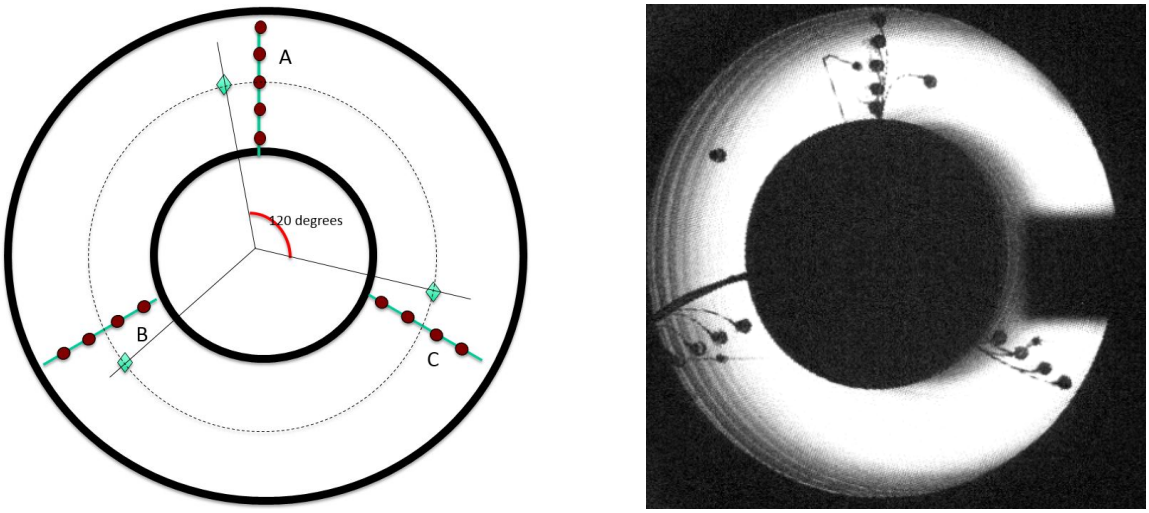

(a) Schematic detailing probe orientation and spacing of the three probe lines.

(b) Photograph of AGI-Engine 6536 operating with probes installed on grid.

Figure 1: Layout of button and Langmuir probes.

The current from each button probe was measured across a 1 kΩ, 25 W resistor. The voltage across each shunt resistor was measured by a 22-channel, 22-bit datalogger connected to a computer. The current density at each probe location was taken to be the ratio of the current measured at the probe to the Faraday probe's physical surface area.

III. Results and Discussion

A. Faraday Probe Measurements

The Faraday button probes were used to track uniformity changes as a function of operating condition. Twelve different operating conditions in total were investigated. Spatial discharge variations as a function of operating condition for four representative power levels (low power) are shown in Fig. 2. Each point represents a probe location on the plots. In general, the probes register similar current densities regardless of location, though none are actually symmetrical about the center of the annulus. Interestingly, at these low power points, the current density is not peaked as one would expect along the cathode axis. At the 1048 W condition, the discharge appears to be the most uniform.

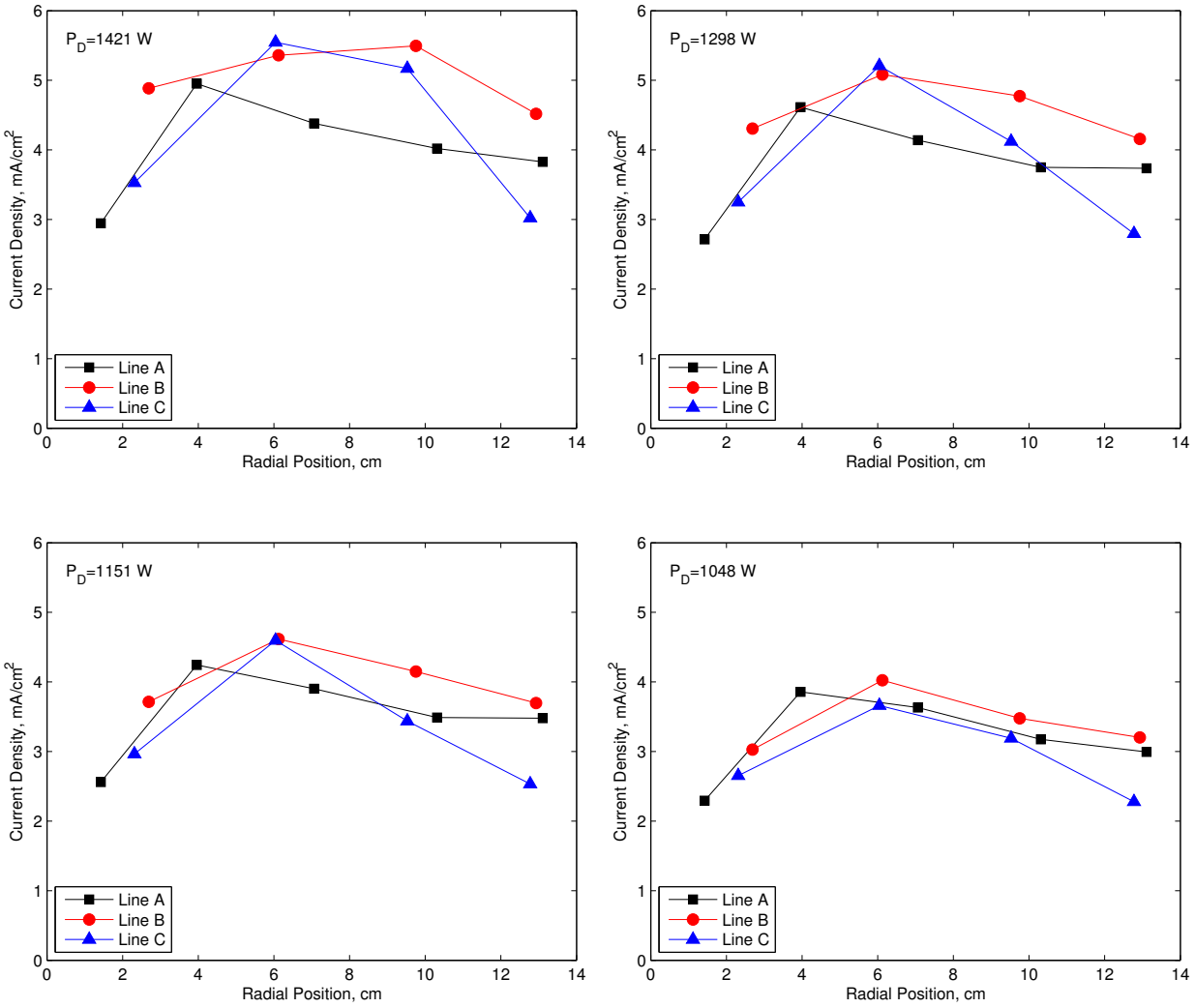

Figure 2: Current density profiles as measured by Faraday button probes.

To better assess discharge uniformity, a percent uniformity parameter was defined. The percent uniformity of the discharge was calculated according to the equation:

$$\% \text{ Uniformity} = \left(1 - \frac{j_{b,max} - j_{b,min}}{j_{b,max} + j_{b,min}}\right) \times 100 \tag{4}$$

where $j_{b,max}$ and $j_{b,min}$ are the maximum and minimum current densities measured by the button probes on a single probe line. This approach to defining uniformity was also previously utilized to assess the AGI-Engine 4208 as well.[3] For this uniformity calculation, the Faraday button probes near the wall of the discharge chamber were excluded. The cusp magnetic field structure tends to insulate plasma from these regions as exemplified by the observed low current densities as shown near the edges in Fig. 2, particularly near the central stalk. The unmagnetized bulk plasma begins several cm from the wall. Figure 3 illustrates the relative magnitude of the magnetic field strength in the annular channel of the engine. The weak field region is apparent in the figure.

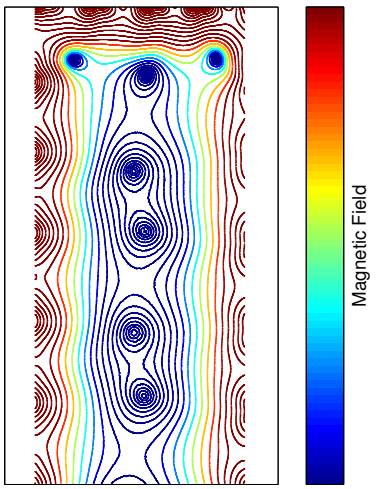

Figure 3: Measured magnetic field profile.

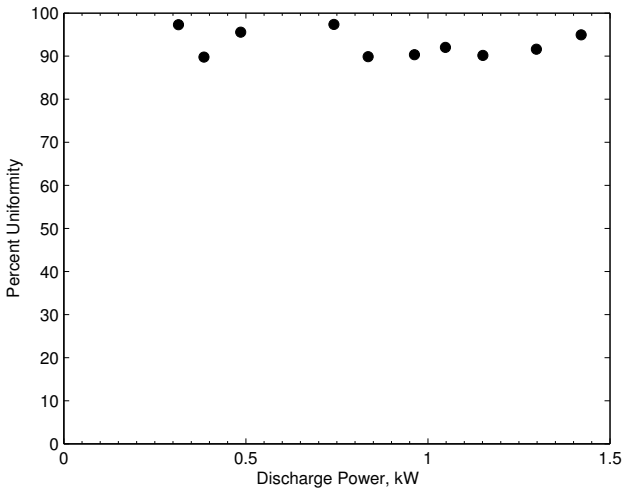

Figure 4: Percent uniformity according to Eq. (4).

The calculated uniformity is shown in Fig. 4. The percent uniformity varies from 89.8% to 97.4%. The discharge is highly uniform despite the azimuthally asymmetric location of the cathode. The maximum current density as a function of discharge power is shown in Fig. 5. Current densities approached 6 mA/cm^2. At discharge powers over 1.1 kW, probe lines "B" and "C" measure current densities that exceed probe line "A". This appears to suggest that with increasing power, the peak in plasma density varies azimuthally. Further spatial mapping is required to determine the overall density spatial structure as a function of azimuthal angle.

B. Langmuir Probe Measurements

The Langmuir probes were used to determine plasma properties at three angular positions. Langmuir probe data was taken for nine of the 12 operating conditions; thermally induced shorting limited the time available to take Langmuir probe data at discharge powers >1.2kW. The electron temperature and ion density are shown in Figs. 6 and 7. The electron temperature was roughly constant at each operating condition within experimental uncertainty (25%). The magnitude of the electron temperature was between 2-6 eV and did not show any trend. An ionization front model would suggest that the highest electron temperature should be near the cathode (0°), falling azimuthally as electron energy is deposited into the xenon gas. This trend

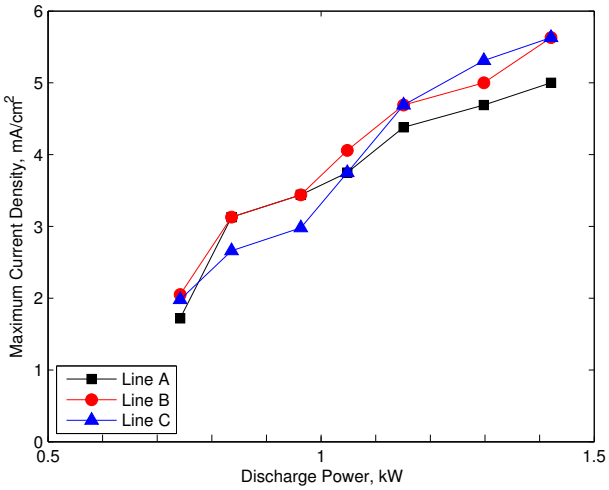

Figure 5: Maximum current density as a function of power for each Faraday probe line.

appears in five of the nine cases plotted in Fig. 6. Notably, this is not the case for the two highest powers investigated (1048 W and 1151 W). in order to precisely determine the trend, a more detailed measurement of the EEDF within the discharge would need to be acquired.

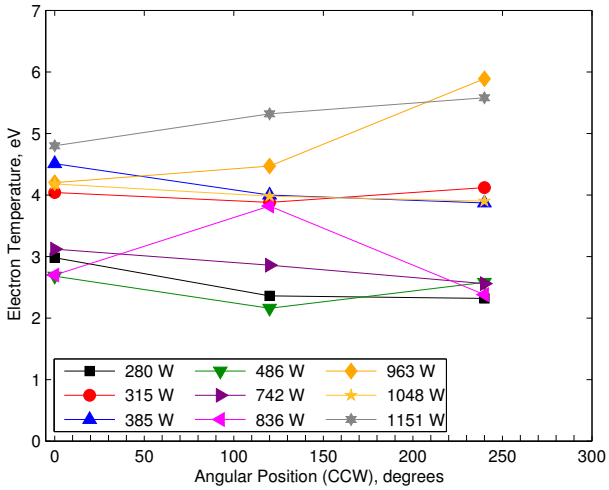

Figure 6: Electron temperature as measured by the three Langmuir probes.

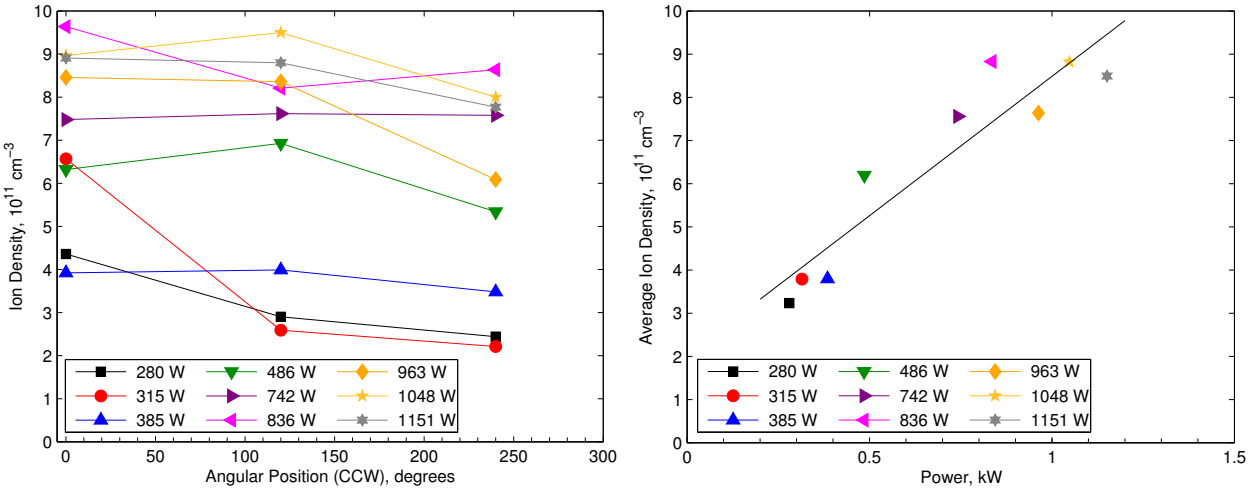

(a) Ion density as a function of angular position.

(b) Ion density as a function of power.

Figure 7: Ion density as measured by the three Langmuir probes.

In general, the magnitude of the ion density increased monotonically with increasing power, as expected. The two exceptions are the 836 W condition, which had a larger than expected ion density, and the 1151 W condition, which had a lower than expected ion density.

C. Fast Camera

The relative high degree of plasma uniformity in the discharge chamber is somewhat surprising given the discharge geometry. It is possible that an instability may be present that enhances electron transport in the azimuthal direction. A Vision Research Phantom v710 fast frame-rate camera was trained on the engine to look for instabilities, which is capable of frame-rates up to 8360 fps at 720p. During steady state engine operation, no instabilities were detected. This data suggests that at least for frequencies less than 10 kHz, no time varying perturbations were observed. Also of interest was the nature of plasma propagation upon startup. It was not clear how the discharge propagated circumferentially to fill the chamber upon startup. The fast camera captured the start up transients. Figure 8 shows the AGI-Engine 6536 during startup. The frame-rate for this data was set at 10000 fps. Plasma forms first near the cathode and then the ionization front propagates azimuthally in both directions. After 1.6 ms, plasma has filled the discharge chamber. Interestingly, one can attribute a crude propagation time given the engine size. This would constitute at best a few hundred m/s for plasma fill time. This time is below that of the ion acoustic speed and is more characteristic of gas dynamic processes rather than plasma effects. However, these images were taken during steady state flow, so filling effects can be discounted. It was postulated that the origin for the high uniformity in the AGI-Engine 4208 was due to drifts—namely the combination of the curvature and $\nabla\vec{B}$ drifts, which occur in the azimuthal direction. The curvature and $\nabla\vec{B}$ drifts are given respectively by the equations:

$$v_C = \frac{mv_\parallel^2}{q\mathbf{B}}\frac{\vec{B}\times\nabla\vec{B}}{\mathbf{B}^2} \tag{5}$$

and

$$v_{\nabla\vec{B}} = \frac{mv_\perp^2}{2q\mathbf{B}}\frac{\vec{B}\times\nabla\vec{B}}{\mathbf{B}^2} \tag{6}$$

where m is the electron mass and $v_\parallel$ and $v_\perp$ are the components of the electron velocity parallel and perpendicular to $\vec{B}$ respectively. These equations can be combined to give the full drift velocity:

$$v_D = \frac{1}{\Omega}\left(\frac{v_\perp^2}{2} + v_\parallel\right)\frac{\vec{B}\times\nabla\vec{B}}{\mathbf{B}^2} \tag{7}$$

where Ω is the cyclotron frequency, $q\mathbf{B}/m$.

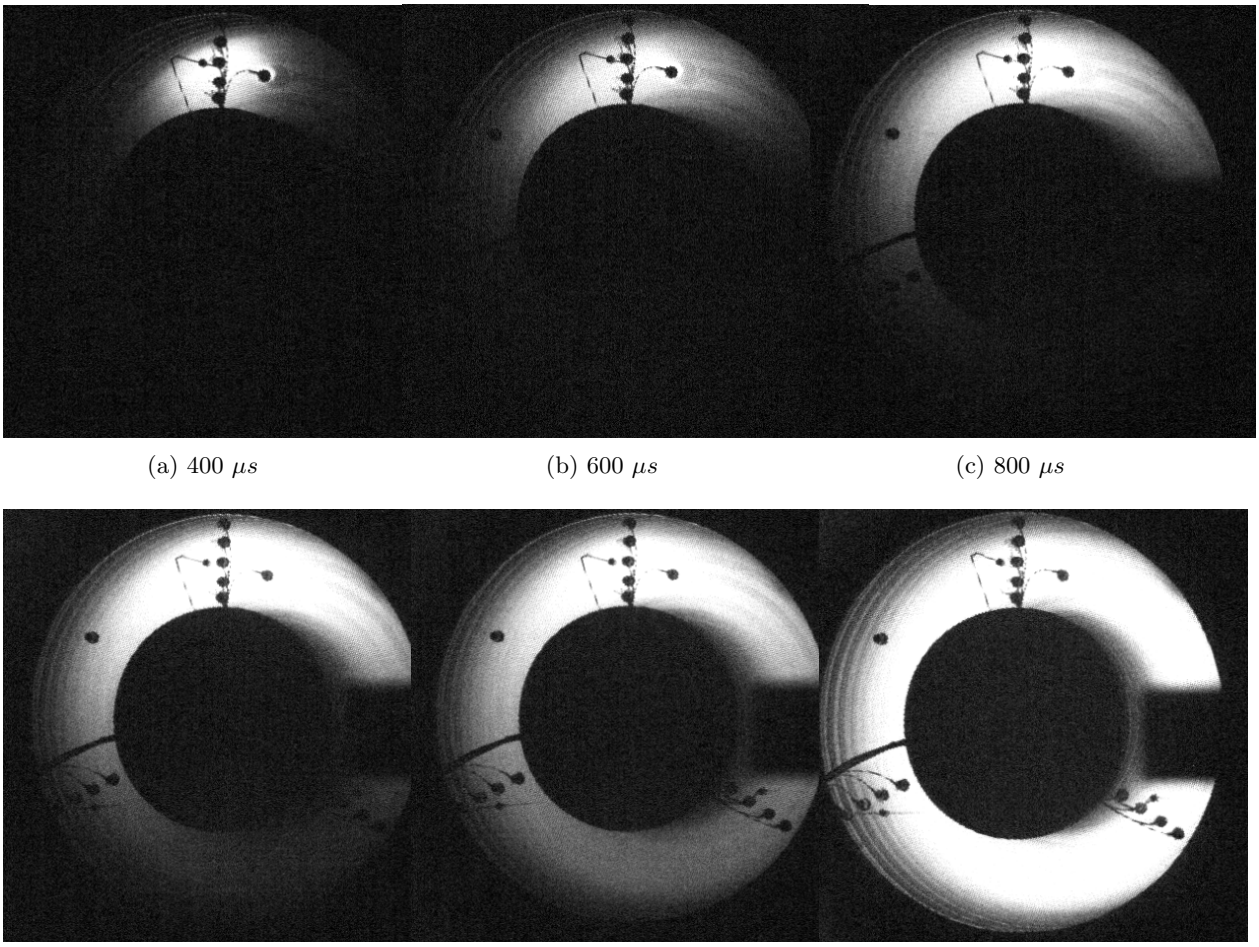

(a) 400 μs (b) 600 μs (c) 800 μs

(d) 1 ms (e) 1.6 ms (f) >10 ms

Figure 8: Fast camera images during engine startup.

Because the fast camera gives one plasma fill time scales, it is possible to determine if the plasma fill time is consistent with the combined curvature and $\nabla \vec{B}$ drifts. Given the average field near the boundary of the "unmagnetized" region, one finds that this drift is of similar magnitude as that measured with the fast camera. This preliminary calculation suggests that rather than instabilities, plasma filling is due to drifts associated with field spatial non-uniformity. More refined measurements are left to future work, but this preliminary data does suggest the importance of drifts in plasma filling. Spatial variations in plasma parameters affect plasma drift velocity and therefore change the spatial density distribution as operating conditions vary.

D. Magnet Burn Lines

Plasma uniformity in a given region is ultimately related to the local magnetic field strength, which essentially establishes loss rates. In order to assess confinement, burn lines at the surface of the plasma-facing magnetic rings on the anode was measured. By burn line, we refer to the plasma generated marks observed to form at the center of each magnet ring due to localized collection. This mark is associated with the leak width at the magnetic cusp. The width of the magnetic burn lines, depicted in Fig. 9, were measured from post-test photographs using ImageJ software. The burn line width was 0.15 mm on the inner magnet rings and 0.90 mm on the outer magnet rings. The inner and outer magnet rings have the same spacing; however, the inner rings have a smaller circumference leading to higher magnetic energy density near the inner magnet rings. The burn line measurements suggest that there is better confinement near the central stalk. This

could lead to preferred diffusion directed towards the outer magnet rings, leading to asymmetrical density profiles similar to those observed along probe lines "A", "B", and "C" in Fig. 2.

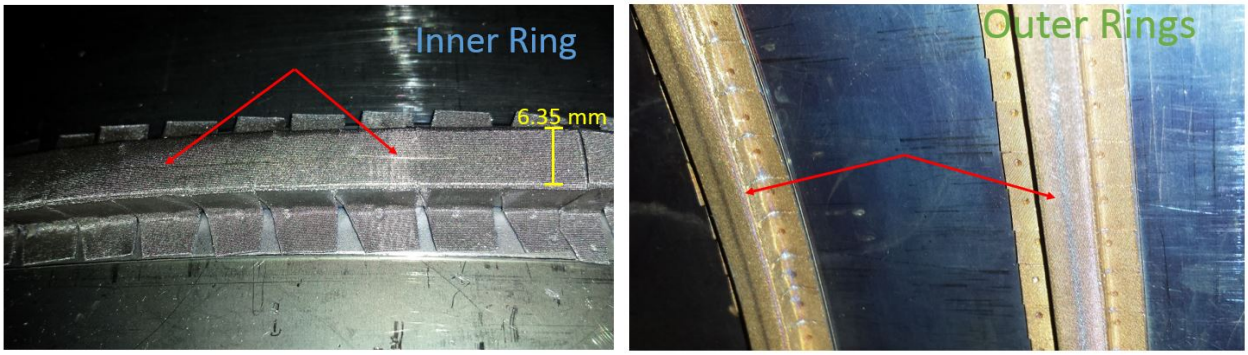

(a) Inner magnet rings.

(b) Outer magnet rings.

Figure 9: Post-test photographs showing the magnet rings and their burn lines.

IV. Conclusion

Preliminary discharge characterization of a 65 cm annular ion engine was carried out at low power. The discharge at low power levels was surprisingly uniform. The degree of uniformity varied slightly with operating condition. Fast camera images of engine startup suggests that possibly the combined curvature/$\nabla\vec{B}$ drift are responsible for observed discharge uniformity. Burn line analysis suggest that slight modification of the field near the central stalk could be used to symmetrize the discharge profile across the annulus. Further discharge characterization at higher power will be necessary to fully understand the dependence of uniformity on power level.

References

[1] Patterson, M. J. and Rawlin, V. K., "Performance of 10-kW Class Xenon Ion Thrusters," *Joint Propulsion Conference*, AIAA Paper 88-2914, 1988.

[2] Patterson, M. J., Foster, J. E., Young, J. A., and Crofton, M. W.,"Annular Engine Development Status," *Joint Propulsion Conference*, AIAA Paper 3892, 2013.

[3] Shastry, R., Patterson, M. J., Herman, D. A., and Foster, J. E., "Current Density Measurements of an Annular-Geometry Ion Engine," *Joint Propulsion Conference*, AIAA Paper 4186, 2012.

[4] Patterson, M. J., Herman, D., Shastry, R., and Van Noord, J., "Annular-Geometry Ion Engine: Concept, Development Status, and Preliminary Performance," *Joint Propulsion Conference*, AIAA Paper 3798, 2012.

[5] Brophy, J. R., "Simulated ion thruster operation without beam extraction," *International Electric Propulsion Conference*, AIAA Paper 90-2655, NASA, 1990.